AIChE Journal
DOI 10.1002/aic.16094

Highly Efficient Methane Reforming over a Low-loading Ru/γ-Al_2O_3 Catalyst in a Pd-Ag Membrane Reactor

David S. A. Simakov[1*] and Yuriy Román-Leshkov[2*]

[1] Department of Chemical Engineering, University of Waterloo, Waterloo, ON N2L 3G1, Canada

[2] Department of Chemical Engineering, Massachusetts Institute of Technology, Cambridge, MA 02139

Natural gas can be reformed to syngas ($CH_4 + H_2O = CO + 3H_2$), at temperatures above 850 °C. Membrane catalytic reformers can provide high CH_4 conversions at temperatures below 650 °C, by separating H_2 from the reactive mixture. Traditional Ni-based catalysts suffer from low activity at low temperatures and deactivate rapidly by coking, particularly at low steam/carbon ratios. In this study, an ultra-low loading (0.15 wt%) Ru/γ-Al_2O_3 catalyst was implemented in a lab-scale membrane reformer, using a supported 5μm Pd-Ag film membrane. Methane conversions above 90% were achieved at 650 °C, 8 bar, and H_2O/CH_4 = 2, 3 with contact times of ca. 10 s. The system generated up to 3.5 mol of ultra-pure H_2 per mol of CH_4 fed, with a maximum power density of 0.9 kW/L. No significant deactivation was observed after 200 h time on stream, even when using low H_2O:CH_4 ratios.

Keywords: *membrane reactor, methane reforming, dry reforming, ruthenium catalyst*

* Correspondence concerning this article should be addressed to D.S.A. Simakov at dsimakov@uwaterloo.ca or Y. Román-Leshkov at yroman@mit.edu.

This article has been accepted for publication and undergone full peer review but has not been through the copyediting, typesetting, pagination and proofreading process which may lead to differences between this version and the Version of Record. Please cite this article as doi: 10.1002/aic.16094

Received: Oct 10, 2017; Revised: Jan 08, 2018; Accepted: Jan 12, 2018

Introduction

The development and widespread use of horizontal drilling and hydraulic fracturing technologies for the extraction of shale gas has drastically increased the availability of natural gas as a cheap feedstock for the energy sector and the chemical industry. The composition of natural gas is variable, but it is mostly composed of CH_4 (usually > 90%), with the rest comprising CO_2, small amounts of ethane, and negligible quantities of longer-chained hydrocarbons and impurities. In the chemical industry, natural gas is converted to synthesis gas via the steam reforming process over Ni-based catalysts.[1] If hydrogen is a desired product rather than syngas (e.g., in ammonia synthesis), additional steps of water gas shift and separation are required.

Steam methane reforming (SMR) is a highly endothermic, reversible process with CH_4 conversion thermodynamically favored at high temperatures and low pressures.[1] The overall SMR process is commonly described by three reactions: reforming to CO, water gas shift, and direct reforming to CO_2, as shown in Eqs. 1-3 below.

$$CH_4 + H_2O = CO + 3H_2 \qquad \Delta H^{\circ}_{298K} = 206.1 \text{ kJ/mol} \tag{1}$$

$$CO + H_2O = CO_2 + H_2 \qquad \Delta H^{\circ}_{298K} = -41.2 \text{ kJ/mol} \tag{2}$$

$$CH_4 + 2H_2O = CO_2 + 4H_2 \qquad \Delta H^{\circ}_{298K} = 164.9 \text{ kJ/mol} \tag{3}$$

The thermodynamics of the SMR process dictate that temperatures above 850 °C are needed to obtain CH_4 conversions above 80% at the elevated pressures (5-20 bar) required in industrial processing units.[1] Dry methane reforming (DMR), although a very well-known reaction, has a lot

of challenges associated with catalyst deactivation and efficient heat supply, as this process is even more endothermic than SMR:[2,3]

$$CO_2 + CH_4 = 2CO + 2H_2 \qquad \Delta H^{\circ}_{298K} = +247.3 \text{ kJ/mol} \qquad (4)$$

However, this process is an attractive alternative for syngas generation because CO_2 is used as an oxidant instead of steam, opening a pathway for CO_2 conversion into synthetic fuels.[4]

Operating at high temperatures and pressures has severe consequences on the stability of (commercially-used) Ni-based catalysts due to excessive coking. Carbon can be deposited in different forms, either encapsulating the catalytic surface, or diffusing into the metallic catalytic phase and forming filamentous carbon (so-called whiskers).[4] Growth of carbon whiskers can eventually result in mechanical disintegration of the catalyst pellets into finer particles, drastically increasing the pressure drop along the reformer. Thermodynamically speaking, carbon formation is less favorable at low temperatures and high steam-to-carbon ratios.[1] As low temperature is not an option, industrial steam reformers are fed with steam-to-carbon ratios close to 3 to suppress the coking, resulting in less efficient operation due to the increased energy demand for excess steam heating and reactive stream dilution.

In order to enable operation at lower temperatures with lower steam-to-carbon ratios, new catalysts need to be developed that simultaneously are highly active, resistant to coking, and low cost. Such catalysts can be based on novel materials (e.g., transition metal carbides)[1] or ultra-low loading formulations of platinum group metals.[5] Yet, the restriction on the CH_4 conversion imposed by the thermodynamics cannot be overcome in a conventional reactor. Fortunately, this limitation can be circumvented by the use of a membrane reactor with *in situ* H_2 separation[6]. In a membrane reformer, the equilibrium is shifted according to Le Chatelier's principle by a

selective removal of H_2 from the reactive stream via a perm-selective membrane (e.g., a Pd-based membrane).[7,8] Recent progress in the development of supported, ultra-thin film Pd alloy membranes allowed for a very significant cost reduction in their production.[9] Due to the high potential for low temperature, highly-efficient reforming applications membrane reactors have attracted significant attention and have been studied theoretically[1,7,10,11] and experimentally.[8,12-20] Importantly, membrane reactors will critically enable low-temperature solar thermal reforming,[9,11,21] allowing for the direct incorporation of renewable energy into the chemical industry production streams via the upgrading of natural gas with sunlight.[1,21] Although a substantial amount of work has been done in this new field, focused studies are required to evaluate the potential of membrane reformers in terms of process efficiency and catalyst stability, in particular using low steam-to-carbon ratios and catalysts with ultra-low metal loadings.

Previously, we reported on the catalytic performance and characterization of an ultra-low loading 0.15wt% Ru/γ-Al_2O_3 catalyst for SMR.[5] Briefly, that study showed that the catalyst was highly active (turnover frequency as high as 40 1/s at 600 °C) with a pronounced optimum in catalytic activity at the 0.15wt% Ru loading, which can be attributed to the optimal Ru nanoparticle distribution. The 0.15wt% Ru/γ-Al_2O_3 catalyst also featured excellent stability at low steam-to-carbon ratios and high space velocities, making it an attractive option for low-temperature CH_4 reforming. Membrane-assisted reforming allows reaching nearly complete CH_4 conversions at 600 °C and elevated pressures, conditions which are favorable for membrane reformers as opposed to conventional operation.[9]

In this study, we investigated the SMR reaction in a lab-scale (6 in. length, 0.5 in. OD) membrane reactor under low temperature conditions using the 0.15 wt% Ru/γ-Al_2O_3catalyst.[5]

The supported 5μm Pd-Ag film membrane was used for *in situ* H_2 separation, allowing for methane conversions well above the equilibrium values to be reached, and generating up to 3.5 mol of ultra-pure H_2 per mol of CH_4 fed. The maximum power density of this lab-scale unit was 0.9 kW/L (electrical power equivalent). No significant deactivation was observed after200 h on stream. The feasibility of using this system for low steam/carbon ratios (S/C=1 or 2) and for dry (CO_2) reforming conditions was also investigated.

Experimental

The 0.15wt% Ru/γ-Al_2O_3 catalyst preparation is described in detail elsewhere[5]. Briefly, $RuCl_3 \times H_2O$ (38 % Ru, Alfa Aesar) was dissolved in acetone (99.5 % purity, Alfa Aesar), and the high surface area aluminum oxide support (γ-Al_2O_3, 220 m^2/g, 1/8 in. pellets, Alfa Aesar) was crushed and sieved to 250-425 μm particles and then added to the solution. The resulting slurry was placed in an ultrasonic bath (Branson 5510) in a glass vial for 30 min. After sonication, acetone was evaporated at 55 °C. The resulting catalyst precursor (250-425 μm particles impregnated with $RuCl_3$) was directly loaded into the reactor so that the heat treatment required to decompose $RuCl_3$ forming γ-Al_2O_3-supported Ru nanoparticles was carried out *in situ*, under the flow of H_2.

The concept of the membrane reactor used in experiments is shown in Figure 1a. The driving force for H_2 separation is the difference between the partial pressure of H_2 in the membrane interior ($p_{H_2,M}$) and that in the catalytic bed, which is a product of the packed bed H_2 mole fraction and pressure (P). The H_2 permeation mechanism is the temperature-activated atomic diffusion through the Pd-Ag film, as described by Sieverts' law[9,21] (J_{H_2}, A_{H_2}, and E_{H_2} are the membrane flux, permeability, and activation energy, respectively):

$$J_{H_2} = A_{H_2} \exp\left(-\frac{E_{H_2}}{R_g T}\right)\left(\sqrt{y_{H_2} P} - \sqrt{p_{H_2,\mathrm{M}}}\right) \quad (5)$$

Sweep gas can be applied to lower the H_2 partial pressure in the membrane interior, Figure 1a. Inert gases which are typically used for that purpose in a laboratory environment can be replaced by steam for practical applications[9]. The lab-scale unit used in experiments is shown in Figure 1b. The upper left and right panels show the membrane (REB Research & Consulting, (5 μm Pd-Ag film/Inconel, 6 in. long × 1/8 in. OD × 0.003 in. wall) and the catalyst particles, respectively. The entire unit is shown in the lower panel. The weight of the catalytic bed loaded in the active part (6 in. long × ¼ in. OD × 0.035 in. wall) surrounding the membrane (lower panel in Figure 2b) was 8 g. Intraparticle and interparticle transport limitations were ruled out using the following criteria for heat and mass transfer resistances:[10,22]

$$\phi^2 \equiv \frac{k_{SMR} d_p^2}{4 D_e} << 1 \qquad \text{(intraparticle mass transfer)}$$

$$\frac{\varepsilon \rho_g \left|\Delta H_{SMR}\right| k_{SMR} d_p^2}{4 k_s T} << \frac{0.75 T R_g}{E_a} \qquad \text{(intraparticle heat transfer)}$$

$$\frac{k_{SMR} d_p}{2 y_{CH_4,f} k_c} << 0.15 \qquad \text{(interphase mass transfer criterion)}$$

$$\frac{\varepsilon \rho_g \left|\Delta H_{SMR}\right| k_{SMR} d_p}{2 h_{gs} T} << \frac{0.15 T R_g}{E_a} \qquad \text{(interphase heat transfer criterion)}$$

$$k_{SMR} = k_{ref} \exp\left[\frac{E_a}{R_g}\left(\frac{1}{T_{ref}} - \frac{1}{T}\right)\right] \quad (6)$$

Apparent activation energy (E_a = 72.5 kJ/mol) and reference reaction rate constant (k_{ref} (674 K) = 0.29 1/s) values were extracted from kinetic data previously obtained for the 0.15wt% Ru/γ-Al_2O_3 catalyst.[5] All calculations showed that under the reaction conditions investigated, no mass or heat transfer limitations were present.

Reactor performance evaluation was carried out using a continuous flow system controlled and monitored by a computer with a continuous data recording (LabVIEW, National Instruments Corporation), as depicted in Figure 2. The reactor was heated in an electric furnace (model 3210, Applied Test Systems, Inc.) equipped with a temperature controller (model 68900-10, Digi-Sense). A K-type thermocouple (OMEGA Engineering, Inc.) was placed inside the reactor tube in a contact with the catalyst bed, Figure 1b. Analog-to-digital/digital-to-analog converters (model NI USB-9263, NI USB-9215, NI USB-9211, NI cDAQ-9184, National Instruments Corporation) were used to control gas flow via mass flow controllers (model 5850TR, Brooks Instrument) and water supply via a syringe pump (model NE-8000, New Era Pump Systems Inc., USA), and to monitor flow rates and temperature continuously. Pressure was regulated using a back pressure regulator (model 44-2363-24, TESCOM Corporation, USA). Concentrations of CH_4, CO and CO_2 were measured using an infrared analyzer (model IR-208, Infrared Industries, Inc., USA) on a dry basis, after removal of water condensate by a water trap (model NAFM4000-N02, SMC Corporation of America) and residual humidity by a column packed with silica gel pellets (2-5 mm, Sigma Aldrich), Figure 2.

The catalyst was first reduced *in situ* in flowing H_2 (200 mL/min) by ramping to 600 °C with a heating rate of 10 °/min with a subsequent isothermal step at 600 °C for 1 h. The feed stream was then switched to a mixture of CH_4 and H_2O. Gas hourly space velocity (GHSV) is defined as

the ratio of the volumetric flow rate (at room temperature, atmospheric pressure) of carbon feed (either CH_4 for steam reforming or $CH_4 + CO_2$ for dry reforming) and the catalyst bed weight:

$$GHSV = \frac{Q_{C,f}}{W_c} \tag{7}$$

The reactor outlet flow rate ($Q_{r,out}$) and the membrane permeate flow rate ($Q_{H_2,out}$) were measured with a soap film flowmeter installed after the water removal segment (Figure 2). It was verified that the membrane outlet streams did not contain any CO, CO_2 or CH_4, using the infrared gas analyzer (we also confirmed before and after the experiments that the membrane is only permeable to H_2). Conversions (X_{CH_4} and X_{CO_2}), selectivity to CO formation (S_{CO}), and H_2 yield (Y_{H_2}) were calculated as follows (y_{CH_4}, y_{CO_2}, and y_{CO} stands for molar fractions measured by the infrared analyzer, Figure 2):

$$X_{CH_4} = \frac{Q_{CH_4,f} - y_{CH_4} Q_{r,out}}{Q_{CH_4,f}} \tag{8}$$

$$X_{CO_2} = \frac{Q_{CO_2,f} - y_{CO_2} Q_{r,out}}{Q_{CO_2,f}} \tag{9}$$

$$Y_{H_2} = \frac{Q_{H_2,out}}{Q_{CH_4,f}} \tag{10}$$

Results and Discussion

Membrane reactor performance and stability

Before starting reforming experiments, the membrane permeability was estimated using a standard technique, Figure 3. Pure H_2 was fed to the empty reactor (without catalyst) heated to different temperatures under different pressures, while measuring the H_2 flow rate at the

membrane interior outlet (kept at atmospheric pressure). As it can be seen from the H_2 flux plotted versus the difference of pressure square roots, the membrane flux followed Eq. 5, as expected. The activation energy and permeability coefficient were determined using the logarithmic from of Eq. 5, as it is shown in Figure 3 (right panel). The estimated values were E_{H_2} = 22.4 kJ/mol and A_{H_2} = 1.81 mol/(m^2 s bar$^{0.5}$).

The reactor performance in terms of CH_4 conversion (X_{CH_4}), selectivity to CO (S_{CO}), and H_2 yield (Y_{H_2}) is shown in Figure 4 (recorded after 50 and 160 h on stream). The catalytic bed fed with a molar ratio of H_2O/CH_4 = 2 was kept at 650 °C, 8 bar on the membrane exterior and atmospheric pressure in the membrane interior. The membrane was swept with N_2 at 200 mL/min. Methane conversion above 80% was achieved at a GHSV < 400 mL/(g h), which is well above the equilibrium conversion value of 41% in a conventional reactor at this temperature and pressure.

The effect of H_2 separation on CO selectivity is also clearly manifested in the membrane reactor, wherein CO selectivity values as low as 10% were obtained at relatively low space velocities. Note that a GHSV = 50-500 mL/(g h) corresponds to contact times of ca. 1-10 s. As expected, the H_2 separation-induced shift in conversion and selectivity vanishes at higher space velocities due to the transport limitation imposed by the membrane permeability.[10]

The lower panel in Figure 4 shows the H_2 flux (defined as the separated H_2 flow rate in cm^3/min per unit of membrane area in cm^2). The observed flux dependence on space velocity is agreement with typical membrane reactor operation,[10] strengthening the above conclusion regarding the membrane transport-limited conversion enhancement. Specifically, at low space velocities (contact time of ca. 10 s), an H_2 yield of as high as 3.5 is achieved, which is near the

maximum value of 4 with no CO formation as expressed in Eq. 3. Note that the H_2 yield in a conventional reactor will be lower than 2 according to the chemical equilibrium. As the space velocity increases, the conversion decreases and so does the H_2 yield, given that less H_2 is produced in the catalytic bed, resulting in lower H_2 partial pressure and a lower rate of H_2 separation (see Eq. 5). The membrane reactor performance was stable over 160 h time on stream, with only minor changes detected between the performance evaluated after 50 and 160 h (Figure 4).

The maximal H_2 flux attained under the conditions listed in Figure 4 was ca. 10 $cm^3/(cm^2$ min). Substituting the previously estimated parameters E_{H_2} and A_{H_2} (Figure 3) into Eq. 5 gives J_{H_2} = 20 $cm^3/(cm^2$ min) for same temperature and pressure, assuming y_{H_2} = 0.6 (70% conversion, see upper panel in Figure 4) and $p_{H_2,M}$ = 0.5 (dilution with sweep gas). The reason for lower membrane flux obtained under reaction conditions could be concertation polarization.[20]

The dependence of conversion, flux, and H_2 yield on space velocity shown in Figure 4 is characteristic of membrane reformers and similar results were reported with a Ni-based catalyst.[10] However, using the highly active Ru-based catalyst could be beneficial at lower temperatures (the Ru-based catalyst used in the current study has much lower activation energy than the Ni-based catalyst, 72.5 kJ/mol[5] vs. 243.9 kJ/mol[10]). Generally speaking, membrane reactor performance can be represented as a product of the Damköhler and membrane Peclet numbers that is the reaction rate-to-separation rate ratio (should be kept high to insure that the reactor is not reaction rate-limited).[10] This ratio depends exponentially on the difference between the membrane and catalyst activation energies (A_{SR} is the reaction rate constant frequency factor for steam reforming):[10]

$$Pe_M Da_{SR} = \frac{reaction\ rate}{separation\ rate} \sim \frac{A_{SR}}{A_{H_2}} \exp\left(\frac{E_{H_2} - E_{SR}}{R_g T}\right) \quad (11)$$

Effect of space velocity and steam-to-carbon ratio

The effect of feed steam-to-carbon ratio on the reactor performance over the range of space velocities is shown in Figure 5. For relatively low space velocities, both conversion and selectivity strongly deviate from their equilibrium values for all free steam-to-carbon ratios. While conversion drops with decreasing steam-to-carbon ratio, the enhancement is still very significant allowing CH_4 conversions as high as 70% as compared to the equilibrium value of 30%. Low steam-to-carbon ratio operation can be advantageous when it is required to produce syngas (a mixture of CO and H_2). At high steam-to-carbon ratios, the equilibrium is shifted towards very low CO selectivity, which is more favorable for H_2 generation with CO_2 as a by-product. The characteristic behavior of the membrane reactor, with conversion declining with space velocity approaching equilibrium values,[10] were observed for all the steam-to-carbon ratios tested.

Figure 6 shows the percentage conversion enhancement and corresponding H_2 yield for several S/C ratios. For GHSV < 1000 mL/(g h), the conversion enhancement was more than 50%, attaining 70-150% enhancement at low space velocity (left panel in Figure 6). For steam-to-carbon ratios of S/C = 2 and 3 it was possible to achieve H_2 yields higher than 3 at GHSV < 400 mL/(g h), while for S/C = 1 the H_2 yield ranged between 1 and 2. These data demonstrate that, in principle, it should be possible to mix the membrane outlet stream (extra-pure H_2) with the catalytic bed outlet stream, producing syngas with targeted H_2/CO ratios. Alternatively, the ultra-pure H_2 stream is amenable for small-to-medium scale or on board fuel cell applications.[7,20]

Power density and cost considerations

The use of a Pd-Ag alloy as a membrane separation film material and Ru as a catalytically active phase suffers from relatively high costs compared to a conventional reforming unit. However, the use of a supported, 5 μm thick film and ultra-low Ru loading can lower the price significantly. Another important consideration is compactness, which is of particular importance for on-site and on-board applications. In this section, the membrane reactor power density and cost (Figure 7) are evaluated based on the obtained experimental data. To calculate the power density, it is assumed that the H_2 generated by the reactor is fed to a fuel cell stack:[9,10]

$$P = \frac{\eta_{FC} \Delta G_{FC} F_{H_2,out}}{V_r} \quad (12)$$

In the equation above, η_{FC} is the fuel cell efficiency (η_{FC} = 0.6 assumed), ΔG_{FC} is the Gibbs free energy of the H_2 oxidation reaction, $F_{H_2,out}$ is the membrane outlet H_2 molar flow rate, and V_r is the reactor volume. In the corresponding cost calculation (right panel in Figure 7), only the price of Pd (it is assumed that the membrane separation film is Pd, not Pd-Ag) and Ru were considered, as the cost of other materials (alumina and stainless steel) will be negligible. The reactor contained 12 mg of Ru (0.02 $) and ca. 100 mg of Pd (2 $). Note that, due to the ultra-low metal loading, the cost of catalyst is negligible as compared the cost of membrane.

The power density achieved in the examined lab-scale unit (left panel in Figure 7) was high and comparable to a typical power density of fuel cells (0.1-1 kW/L). Therefore, adding such a unit to supply H_2 for a fuel cell stack (using CH_4 as a feed rather than H_2) will not result in a significant increase in the total system volume. As expected, power density, which is proportional to the H_2 production rate, Eq. 12, increases with space velocity, achieving power densities as high as 0.9 kW/L. The corresponding cost (a product of power density and the

reactor cost per liter) is shown in the right panel of Figure 7. The cost is moderately high at low space velocities, but drops rapidly as the reactor throughput increases, attaining ca. 150 $/kW, which is comparable to the price of fuel cells. Therefore, capital cost investment could be low.

Combined dry-steam reforming

Dry (CO_2) methane reforming, Eq. 4, has recently attracted renewed attention due to the potential to use CO_2 as a carbon source for the generation of renewable synthetic fuels and chemicals[4]. A number of experimental studies on performing the DMR reaction in a Pd membrane reactor have been published in recent years.[12-14,16,17,19] However, reported conversion enhancements due to H_2 separation were rather minor, especially as compared to reported conversion enhancement achievable in membrane reactors for SMR[8,10] (also see Figures 4-6). As such, typical CH_4 and CO_2 conversions values did not exceed 50%, which is close to equilibrium. Despite the apparent potential for CO_2 utilization, to date, the DMR is not currently used neither for H_2 nor syngas production in either membrane or conventional reactor.[23] The main bottlenecks include undesired reactions, such as the reverse water gas shift (RWGS, the reverse reaction in Eq. 2 that consumes H_2),[23] and extensive carbon formation under dry reforming conditions,[1] which affects not only the catalyst but also the Pd membrane.

Here, we attempted to perform combined dry-steam CH_4 reforming, with the addition of water aimed to suppress coke formation. The results are presented in Figure 8, showing CH_4 and CO_2 conversions with and without membrane (upper panel) and number of moles of H_2 separated

and CO_2 consumed per mole of CH_4 fed (lower panel). CH_4 conversion values were improved by ca. 50% over CO_2/CH_4 feed ratios ranging from 1-2.

However, CO_2 conversions were low due to competing SMR and RWGS reactions. The reactor performance in terms of H_2 production was rather poor (lower panel in Figure 8). Only 1.5 moles of H_2 were produced per mole CH_4 fed at the feed ratio of $CO_2/CH_4 = 1$ and this number declined significantly for higher CO_2/CH_4 feed ratios. Altogether, our preliminary findings indicate that performing combined dry-steam reforming in a membrane reactor is a challenging task, which is in line with previous findings reported in the open literature.[23]

Conclusion

The 0.15wt% Ru/γ-Al_2O_3 catalyst was successfully implemented for methane steam reforming carried out in a lab-scale, 5 μm Pd-Ag Inconel-supported film membrane reactor. Conversions well above the equilibrium were achieved for feed steam-to-carbon ratios ranging from 1-3. The conversion enhancement was as high as 50-150% for contact times of ca. 1-10 s. Methane conversions above 90% were achieved at 650 °C, 8 bar, and $H_2O/CH_4 = 2{,}3$ with contact times of ca. 10 s (equilibrium conversion is 40-50%).

The conversion was not limited by the catalyst activity, being restricted by the membrane separation ability, with the stable membrane performance over total 400 h on stream, including operation with low steam-to-carbon ratios of 1 and 2, and combined dry-steam reforming. Performing methane dry reforming is challenging due to undesired reactions and risk of catalyst and membrane deactivation by coking. For the membrane-assisted methane steam reforming, power densities of up to 0.9 kW/L (fuel cell equivalent) were obtained. Our price estimations

indicated that a reformer cost as low as $100/kW is achievable due to the ultra-low metal loading of the catalyst.

Acknowledgments

The authors highly appreciate and acknowledge the support of King Fahd University of Petroleum and Minerals through the research grant # R12-CE-10 offered by KFUPM-MIT Clean Water and Clean Energy Research Collaboration Center.

Literature Cited

1. Simakov DSA, Wright MM, Ahmed S, Mokheimer EMA, Román-Leshkov Y. Solar thermal catalytic reforming of natural gas: a review on chemistry, catalysis and system design. *Catal Sci Technol.* 2015;5:1991–2016.
2. Ozkara-Aydinoglu S. Thermodynamic equilibrium analysis of combined carbon dioxide reforming with steam reforming of methane to synthesis gas. *Int J Hydrogen Energy.* 2010;35:12821-12828.
3. Usman M, WanDaud WMA, Abbas HF. Dry reforming of methane: Influence ofprocess parameters - A review. *Renew Sustain Energ Rev.* 2015;45:710–744.
4. Simakov DSA. *Renewable Synthetic Fuels and Chemicals from Carbon Dioxide*: Springer International Publishing; 2017.
5. Simakov DSA, Luo HY, Román-Leshkov Y. Ultra-low loading Ru/γ-Al_2O_3: A highly active and stable catalyst for low temperature solar thermal reforming of methane. *Appl Catal B: Environ.* 2015;168-169:540-549.
6. DeFalco M, Marrelli L, Iaquaniello G. *Membrane reactors for hydrogen production processes*: Springer; 2011.
7. Simakov DSA, Sheintuch M. Design of a thermally balanced membrane reformer for hydrogen production. *AIChE J.* 2008;54:2735-2750.
8. Simakov DSA, Sheintuch M. Experimental optimization of an autonomous scaled-down methane membrane reformer for hydrogen generation. *Ind Eng Chem Res.* 2010;49:1123–1129.
9. Said SAM, Simakov DSA, Waseeuddin M, Roman-Leshkov Y. Solar molten salt heated membrane reformer for natural gas upgrading and hydrogen generation: A CFD model. *Solar Energy.* 2016;124:163–176.
10. Simakov DSA, Sheintuch M. Model-based optimization of hydrogen generation by methane steam reforming in autothermal packed-bed membrane reformer. *AIChE J.* 2011;57:525-541.
11. Said SAM, Simakov DSA, Mokheimer EMA, et al. Computational fluid dynamics study of hydrogen generation by low temperature methane reforming in a membrane reactor. *Int J Hydrogen Energy.* 2015;40:3158-3169.
12. Galuszka J, Pandey RN, Ahmed S. Methane conversion to syngas in a palladium membrane reactor. *Catal Today.* 1998;46:83-89.

13. Múnera J, Irusta S, Cornaglia L, Lombardo E. CO_2 reforming of methane as a source of hydrogen using a membrane reactor. *Appl Catal A: Gen* 2003;245:383–395.

14. Paturzo L, Gallucci F, Basile A, Vitulli G, Pertici P. An Ru-based catalytic membrane reactor for dry reforming of methane - its catalytic performance compared with tubular packed bed reactors. *Catal Today.* 2003;82:57–65.

15. Simakov DSA, Sheintuch M. Demonstration of a scaled-down autothermal membrane methane reformer for hydrogen generation. *Int J Hydrogen Energy.* 2009;34:8866-8876.

16. Bosko ML, Múnera JF, Lombardo EA, Cornaglia LM. Dry reforming of methane in membrane reactors using Pd and Pd–Ag composite membranes on a NaA zeolite modified porous stainless steel support. *J Membr Sci.* 2010;364:17–26.

17. Faroldi BM, Lombardo EA, Cornaglia LM. $Ru/La_2O_3–SiO_2$ catalysts for hydrogen production in membrane reactors. *Catal Today.* 2011;172:209– 217.

18. Shigarov AB, Meshcheryakov VD, Kirillov VA. Use of Pd membranes in catalytic reactors for steam methane reforming for pure hydrogen production. *Theoretical Foundations Chem Eng.* 2011;45:595–609.

19. Silva FA, Hori CE, daSilva AM, et al. Hydrogen production through CO_2 reforming of CH_4 over $Pt/CeZrO2/Al_2O_3$ catalysts using a Pd–Ag membrane reactor. *Catal Today.* 2012;193:64-73.

20. Patrascu M, Sheintuch M. On-site pure hydrogen production by methane steam reforming in high flux membrane reactor: Experimental validation, model predictions and membrane inhibition. *Chem Eng J.* 2015;262:862–874.

21. Said SAM, Waseeuddin M, Simakov DSA. A review on solar reforming systems. *Renew Sust Energy Rev.* 2016;59:149–159.

22. Mears DE. Tests for transport limitations in experimental catalytic reactors. *Ind Eng Chem Process Des Dev.* 1971;10:541-547.

23. Oyama ST, Hacarlioglu P, Gu Y, Lee D. Dry reforming of methane has no future for hydrogen production: Comparison with steam reforming at high pressure in standard and membrane reactors. *Int J Hydrogen Energy.* 2012;37:10444-10450.

List of Figure Captions

Figure 1. Membrane reactor concept (a) and the lab-scale experimental unit (b). The membrane tube (upper-left panel in Figure 2b) dimensions were 6″ L × 1/8″ OD × 0.003″ W. The catalyst pellet size was 350 μm.

Figure 2. Experimental flow system: AI/AO – analog input/output module (analog-to-digital/digital-to-analog converter), BPR – backpressure regulator, FI – flow indicator (soap film flowmeter), IR – infrared, MFC – mass flow controller, MT – moisture trap (silica gel), PI – pressure indicator, PR – pressure reducer, TC – thermocouple, TI – temperature indicator, WT – water trap.

Figure 3. Membrane permeability test. The measured membrane flux is shown as a function of the pressure square root difference for various temperatures (left panel). A logarithmic plot of Eq. 5 used to estimate the activation energy and permeability coefficient is shown in the right panel.

Figure 4. Membrane reactor performance in terms of CH_4 conversion, selectivity to CO (upper panel) and H_2 flux and yield (lower panel), as a function of space velocity. Solid and dashed lines in the upper panel show the equilibrium conversion and selectivity, respectively. Open and filled symbols show the performance recorded after 50 h and 160 h on stream, correspondingly. Operating parameters: S/C = 2, T = 650 °C, P_R = 8 bar, P_M = 1 bar, Q_{SG} = 200 ml/min.

Figure 5. Effect of the feed steam-to-carbon ratio on CH_4 conversion (left panel) and selectivity to CO (right panel). Equilibrium is shown by solid, dashed, and dotted lines. Operating parameters: S/C = 1-3, T = 650 °C, P_R = 8 bar, P_M = 1 bar, Q_{SG} = 200 ml/min. All measurements were recorded after 100 h on stream.

Figure 6. Conversion enhancement (left panel) and H_2 yield CO (right panel) as a function of space velocity for different feed steam-to-carbon ratios. Operating parameters: S/C = 1-3, T = 650 °C, P_R = 8 bar, P_M = 1 bar, Q_{SG} = 200 ml/min. All measurements were recorded after 100 h on stream.

Figure 7. Membrane reactor power density (left panel) and the corresponding normalized reactor cost (right panel) as a function of space velocity for different feed steam-to-carbon ratios. Operating parameters: S/C = 1-3, T = 650 °C, P_R = 8 bar, P_M = 1 bar, Q_{SG} = 200 ml/min. All measurements were recorded after 100 h on stream.

Figure 8. Combined dry-steam methane reforming. The shift in CH_4 (triangles) and CO_2 (rhombs) conversion in the membrane reactor (MR) as compared to non-membrane reactor (NMR) is shown in upper panel. Number of moles of H_2 separated (triangles) and CO_2 reacted (rhombs) per number of moles of CH_4 reacted. Operating parameters: GHSV = 375 mL/(g h), H_2O/CH_4 = 0.25, T = 650 °C, P_R = 8 bar, P_M = 1 bar, Q_{SG} = 200 ml/min. All measurements were recorded after 50 h on stream.

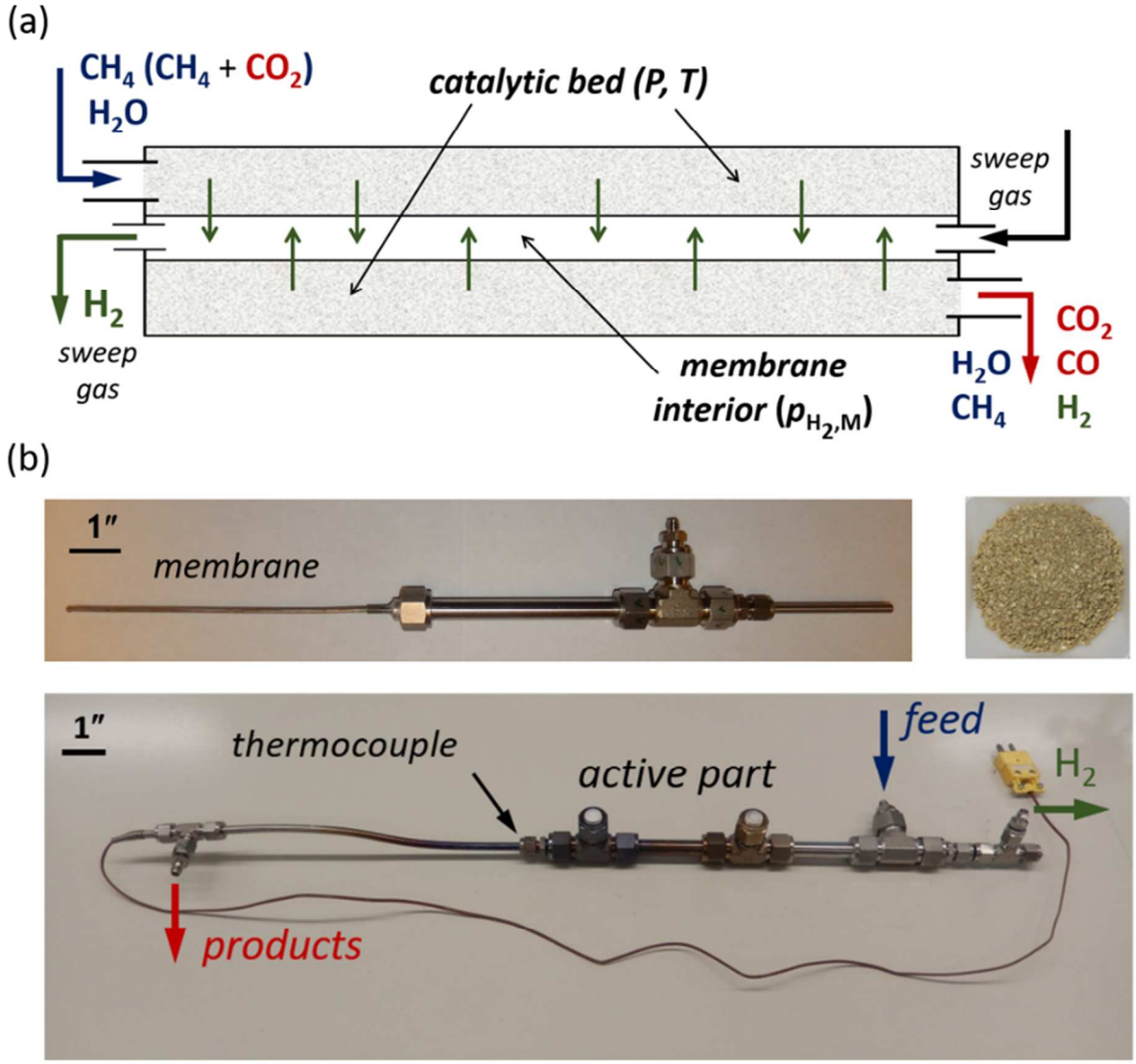

Figure 1. Membrane reactor concept (a) and the lab-scale experimental unit (b). The membrane tube (upper-left panel in Fig. 2b) dimensions were 6″ L × 1/8″ OD × 0.003″ W. The catalyst pellet size was 350 μm.

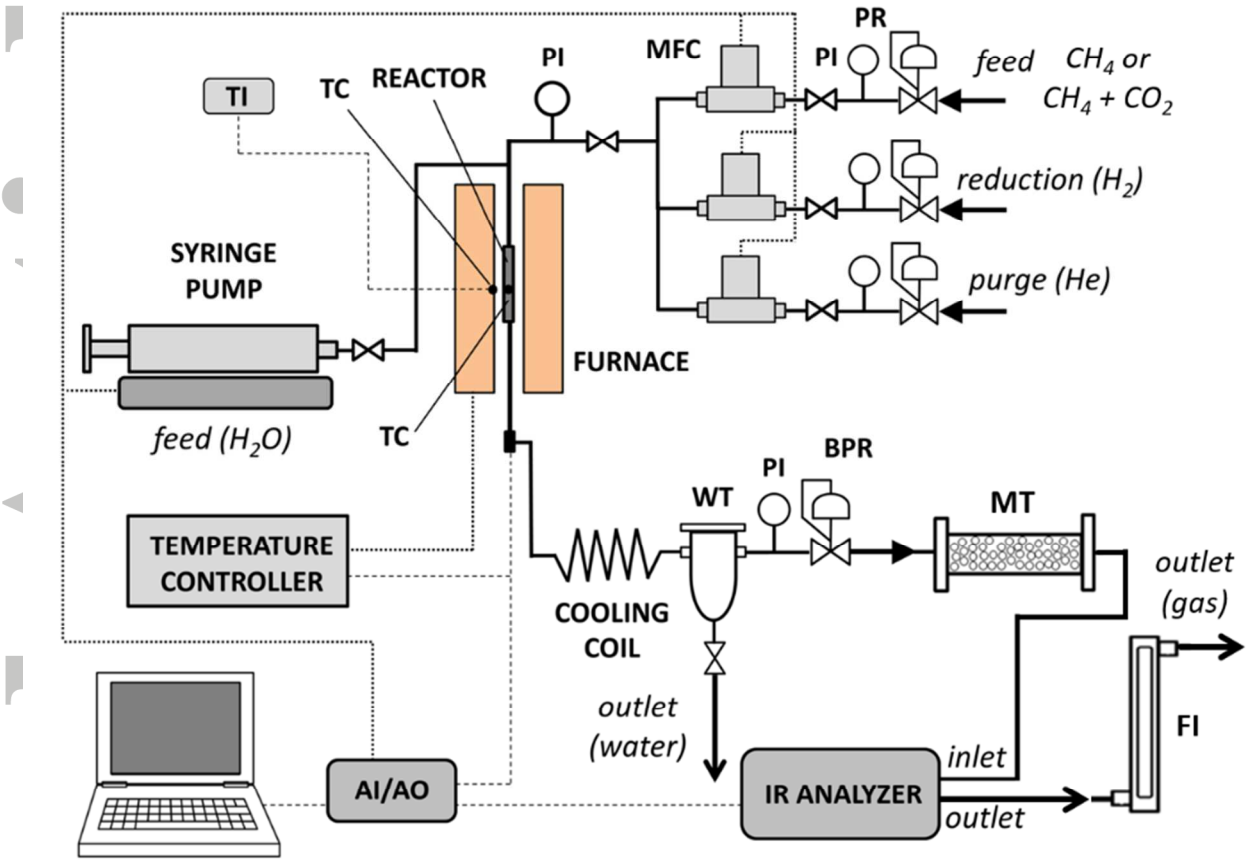

Figure 2. Experimental flow system: AI/AO – analog input/output module (analog-to-digital/digital-to-analog converter), BPR – backpressure regulator, FI – flow indicator (soap film flowmeter), IR – infrared, MFC – mass flow controller, MT – moisture trap (silica gel), PI – pressure indicator, PR – pressure reducer, TC – thermocouple, TI – temperature indicator, WT – water trap.

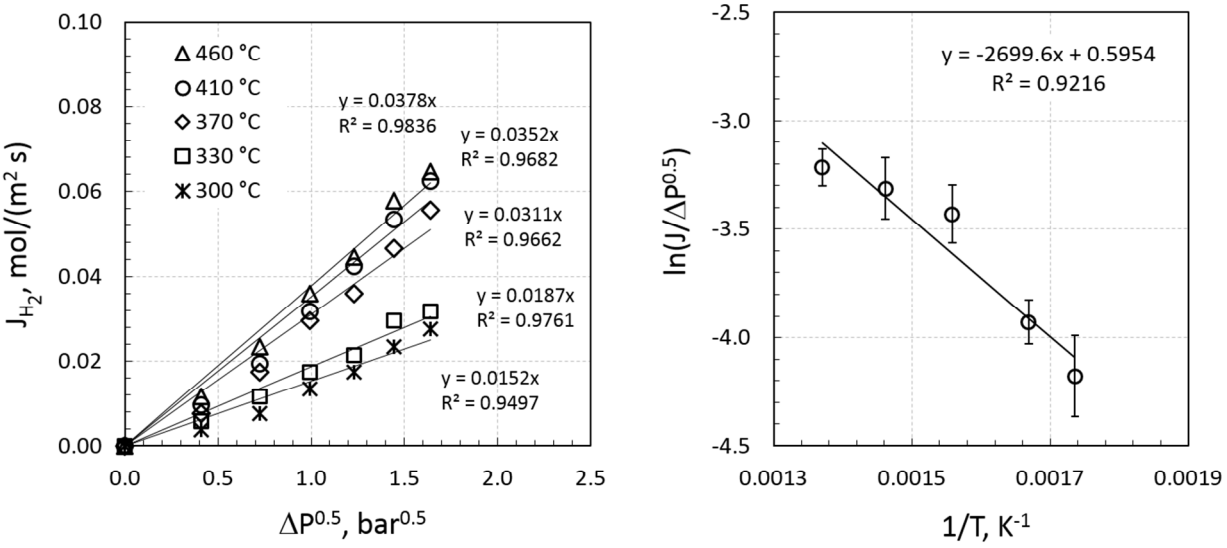

Figure 3. Membrane permeability test. The measured membrane flux is shown as a function of the pressure square root difference for various temperatures (left panel). A logarithmic plot of Eq. (5) used to estimate the activation energy and permeability coefficient is shown in the right panel.

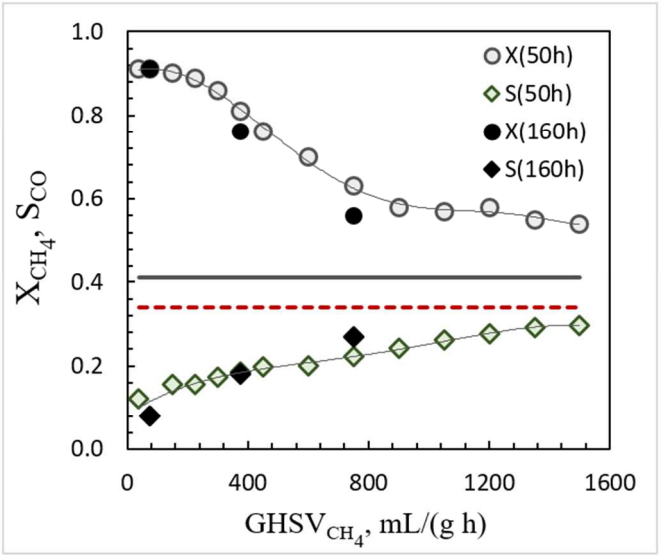

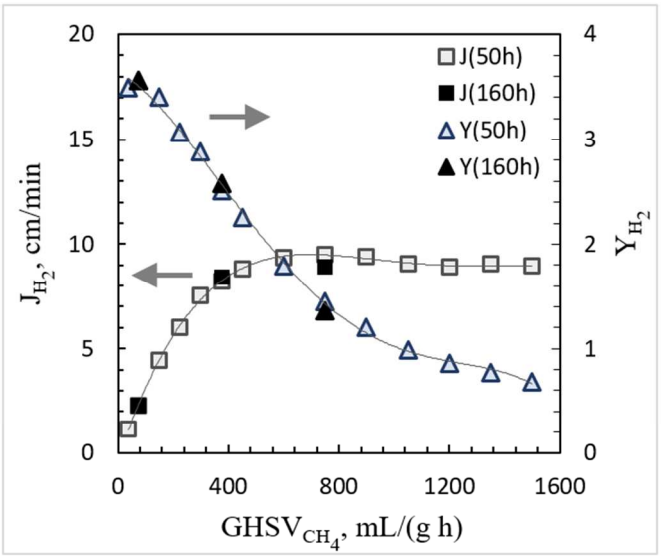

Figure 4. Membrane reactor performance in terms of CH_4 conversion, selectivity to CO (upper panel) and H_2 flux and yield (lower panel), as a function of space velocity. Solid and dashed lines in the upper panel show the equilibrium conversion and selectivity, respectively. Open and filled symbols show the performance recorded after 50 h and 160 h on stream, correspondingly. Operating parameters: S/C = 2, T = 650 °C, P_R = 8 bar, P_M = 1 bar, Q_{SG} = 200

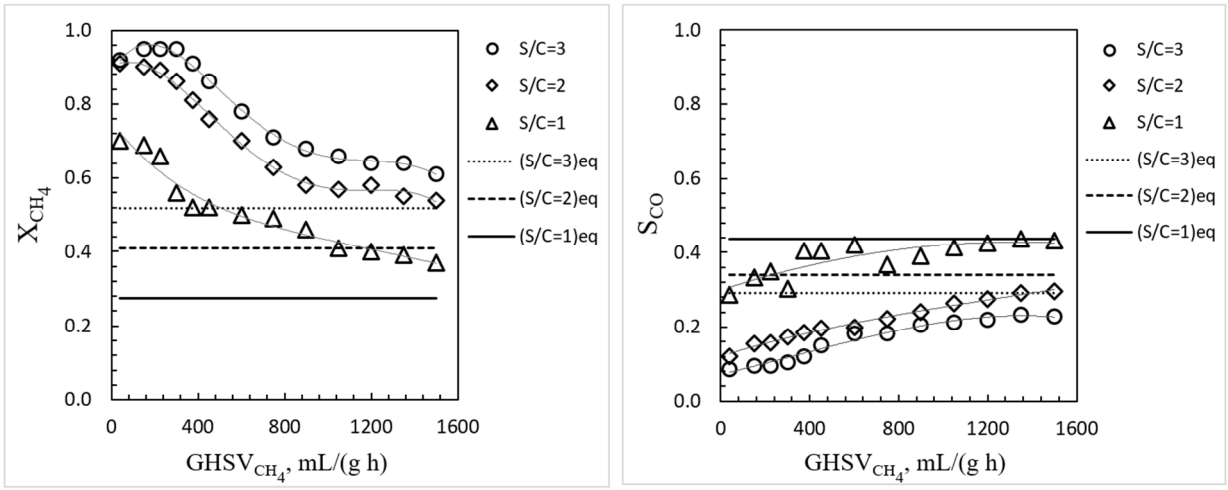

Figure 5. Effect of the feed steam-to-carbon ratio on CH_4 conversion (left panel) and selectivity to CO (right panel). Equilibrium is shown by solid, dashed, and dotted lines. Operating parameters: S/C = 1-3, T = 650 °C, P_R = 8 bar, P_M = 1 bar, Q_{SG} = 200 ml/min. All measurements were recorded after 100 h on stream.

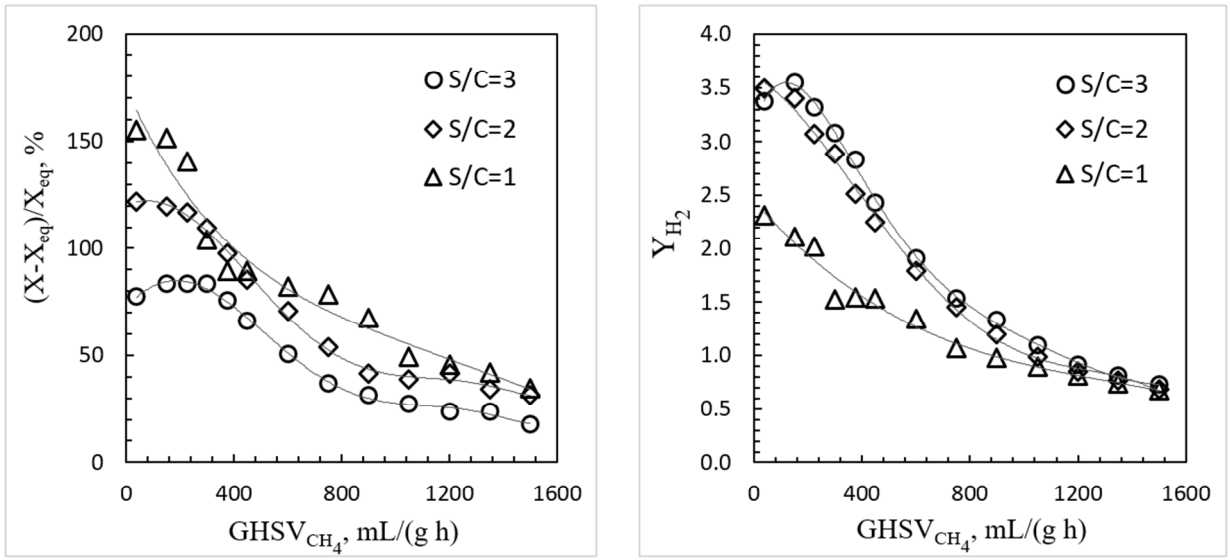

Figure 6. Conversion enhancement (left panel) and H_2 yield CO (right panel) as a function of space velocity for different feed steam-to-carbon ratios. Operating parameters: S/C = 1-3, T = 650 °C, P_R = 8 bar, P_M = 1 bar, Q_{SG} = 200 ml/min. All measurements were recorded after 100 h on stream.

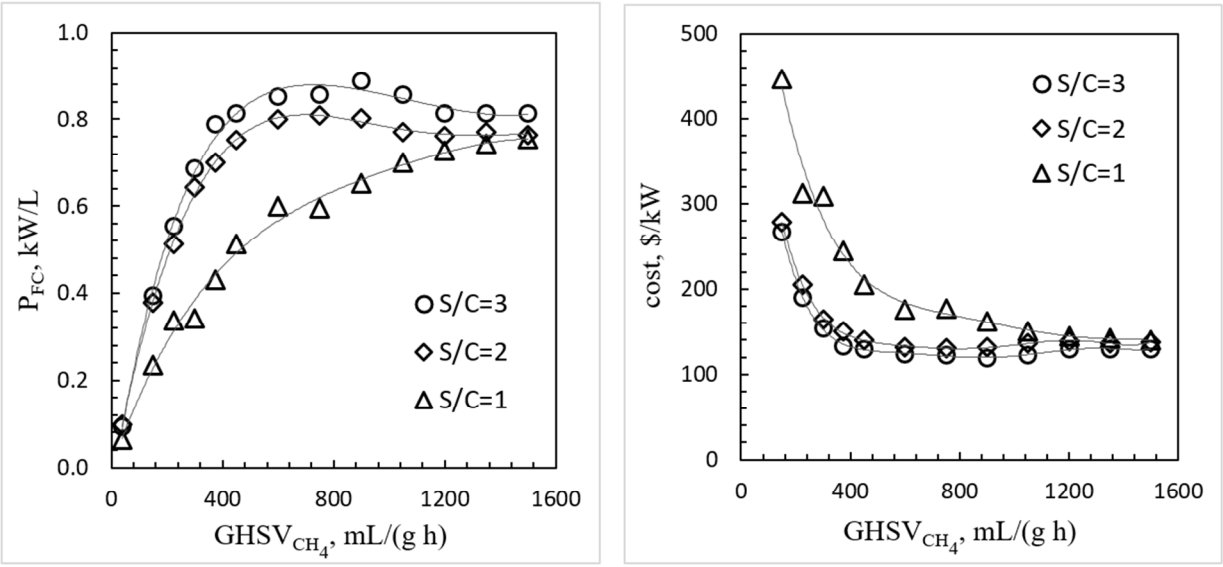

Figure 7. Membrane reactor power density (left panel) and the corresponding normalized reactor cost (right panel) as a function of space velocity for different feed steam-to-carbon ratios. Operating parameters: S/C = 1-3, T = 650 °C, P_R = 8 bar, P_M = 1 bar, Q_{SG} = 200 ml/min. All measurements were recorded after 100 h on stream.

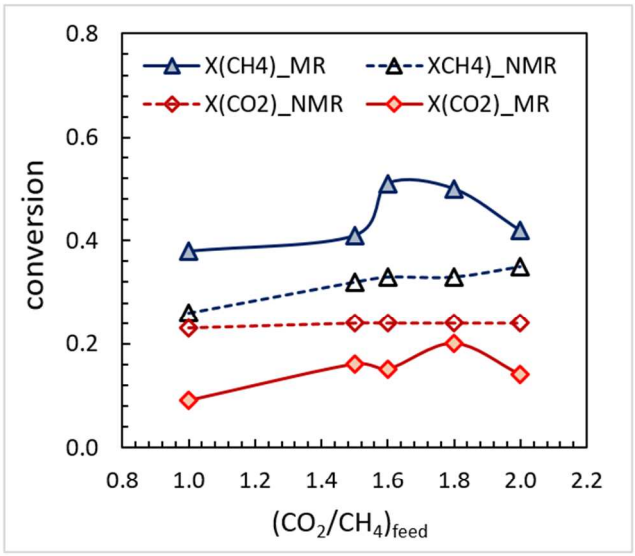

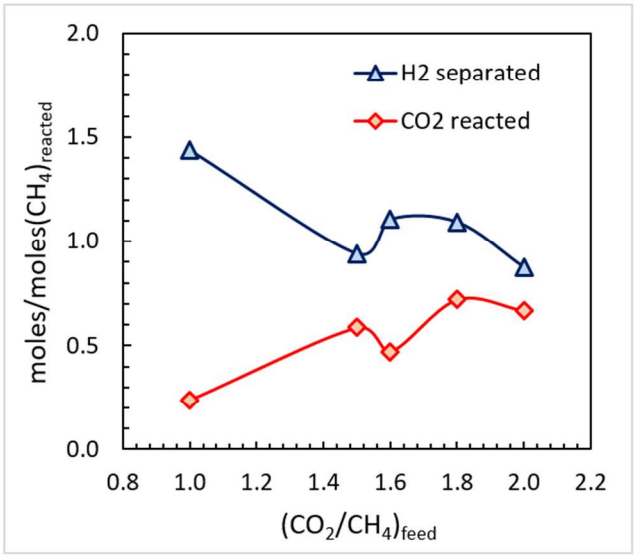

Figure 8. Combined dry-steam methane reforming. The shift in CH_4 (triangles) and CO_2 (rhombs) conversion in the membrane reactor (MR) as compared to non-membrane reactor (NMR) is shown in upper panel. Number of moles of H_2 separated (triangles) and CO_2 reacted (rhombs) per number of moles of CH_4 reacted. Operating parameters: GHSV = 375 mL/(g h), H_2O/CH_4 = 0.25, T = 650 °C, P_R = 8 bar, P_M = 1 bar, Q_{SG} = 200 ml/min. All measurements were recorded after 50 h on stream.